Molecular Biology of the Cell
Vol. 19, 4534–4544, October 2008

Two Microtubule-associated Proteins of *Arabidopsis* MAP65s Promote Antiparallel Microtubule Bundling

Jérémie Gaillard,*† Emmanuelle Neumann,†‡ Daniel Van Damme,§‖ Virginie Stoppin-Mellet,* Christine Ebel,‡ Elodie Barbier,* Danny Geelen,¶ and Marylin Vantard*

*Institut de Recherches en Technologies et Sciences pour le Vivant, Unité Mixte de Recherche, Centre National de la Recherche Scientifique, Centre d'Energie Atomique, Institut de Recherche Agronomique, Université Joseph Fourier, 38054 Grenoble, France; ‡Institut de Biologie Structurale J.-P. Ebel, UMR 5075 CNRS, CEA, Université Joseph Fourier, 38027 Grenoble, France; §Department of Plant Systems Biology, Flanders Institute for Biotechnology, B-9052 Ghent, Belgium; ‖Department of Molecular Genetics, Ghent University, B-9052 Ghent, Belgium; and ¶Department of Plant Production, Ghent University, B-9000 Ghent, Belgium

Submitted April 3, 2008; Revised July 17, 2008; Accepted July 18, 2008
Monitoring Editor: David G. Drubin

The *Arabidopsis* MAP65s are a protein family with similarity to the microtubule-associated proteins PRC1/Ase1p that accumulate in the spindle midzone during late anaphase in mammals and yeast, respectively. Here we investigate the molecular and functional properties of *At*MAP65-5 and improve our understanding of *At*MAP65-1 properties. We demonstrate that, in vitro, both proteins promote the formation of a planar network of antiparallel microtubules. In vivo, we show that *At*MAP65-5 selectively binds the preprophase band and the prophase spindle microtubule during prophase, whereas *At*MAP65-1-GFP selectively binds the preprophase band but does not accumulate at the prophase spindle microtubules that coexists within the same cell. At later stages of mitosis, *At*MAP65-1 and *At*MAP65-5 differentially label the late spindle and phragmoplast. We present evidence for a mode of action for both proteins that involves the binding of monomeric units to microtubules that "zipper up" antiparallel arranged microtubules through the homodimerization of the N-terminal halves when adjacent microtubules encounter.

INTRODUCTION

In higher plant cells, interphase microtubules occur predominantly at the cell cortex as ordered bundles in close association with the plasma membrane. These so-called cortical microtubules (CMTs) play crucial roles in cell morphogenesis (Wasteneys and Fujita, 2006). In rapidly elongating cells, CMTs are linear bundles that are usually transversely oriented relative to the longest cell axis. When cell expansion slows down, the transverse organization is lost and CMTs become oblique (Lloyd, 1994; Dixit and Cyr, 2004). CMTs are highly dynamic and show higher (de)-polymerization rates than interphase mammalian microtubules (Shaw *et al.,* 2003; Dixit *et al.,* 2006). In contrast to animal and yeast microtubules (MTs), CMTs do not emanate from a well-defined nucleating center. Instead, the MT nucleation activity in interphase plant cells mostly occurs at dispersed sites along pre-existing MTs at the cell's cortex (Murata *et al.,* 2005) in a γ-tubulin–dependent manner (Pastuglia *et al.,* 2006). This MT-dependent nucleation results in branching patterns of CMTs (Murata *et al.,* 2005) that are subsequently resolved into coaligned CMTs. After nucleation, the majority of the MTs are released from their nucleation site, move in the cell cortex by a hybrid treadmilling mechanism leading to polymer interactions (Shaw *et al.,* 2003), and are incorporated into bundles (Dixit and Cyr, 2004). Significantly, the CMT bundles are not anchored and consequently both MT ends are dynamic. Thus, the ordered patterns of CMT arrays are not correlated with the patterns of the CMT nucleation sites (Dixit *et al.,* 2006) and depend on a yet-to-be-discovered mechanism.

To accommodate for the transverse network observed in expanding cells, CMTs form bundles. How these bundles are organized is not clear, and for instance, the polarity of CMTs within bundles is not yet solved. Using an in vitro model that provides good access to the cortex combined with the hook decoration of MTs, Tian *et al.* (2004) demonstrated that the MTs in the cortical array are predominantly oriented in a mixed polarity. This organization is in agreement with opposing growth directionalities of green fluorescent protein (GFP)-labeled MTs observed in the cortical array (Chan *et al.,* 2003; Shaw *et al.,* 2003). In contrast, Dixit *et al.* (2006) reported that ~70% of CMTs have the same polarity and that this polar arrangement of CMTs occurs simultaneously with the coalignment of CMTs. This bias toward copolarity might be the net result of sectorial fields of copolymerizing MTs observed in spinning-disk confocal microscopic records (Chan *et al.,* 2007).

This article was published online ahead of print in *MBC in Press* (http://www.molbiolcell.org/cgi/doi/10.1091/mbc.E08–04–0341) on July 30, 2008.

† These authors contributed equally to this work.

Address correspondence to: Marylin Vantard (marylin.vantard@cea.fr).

Abbreviations used: CMT, cortical microtubule; *At*MAP65, *Arabidopsis thaliana* microtubule-associated protein 65; GFP, green fluorescent protein; MT, microtubules.

© 2008 by The American Society for Cell Biology

At the molecular level, putative candidate proteins stimulating the cross-linking of MTs in vitro and in vivo have been identified. They are mainly members of the MT-associated family MAP65s (Smertenko *et al.*, 2004; Wicker-Planquart *et al.*, 2004; Li *et al.*, 2007a). MAP65 proteins are evolutionarily conserved, nonmotor microtubule-associated proteins (MAPs) that in animal and yeast cells accumulate in the spindle midzone during late anaphase to stabilize overlapping antiparallel arranged MTs (Verni *et al.*, 2004; Zhu *et al.*, 2006; Janson *et al.*, 2007). In *Arabidopsis* nine *At*MAP65 family members were identified (Hussey *et al.*, 2002). These all possess a conserved sequence of 16 amino acids located at the C-terminus and coiled-coil sequences with putative protein–protein interaction activity (Schuyler *et al.*, 2003; Verni *et al.*, 2004). Overall sequence identity is poorly conserved, suggesting that *At*MAP65 proteins have adopted separate properties. *At*MAP65-1 is so far the more studied and was shown to colocalize with bundled CMTs and the spindle midzone in anaphase (Van Damme *et al.*, 2004a; Mao *et al.*, 2005a; Smertenko *et al.*, 2006). In vitro, *At*MAP65-1 promotes MT bundling and appears as filamentous cross-bridges regularly spaced along the MT wall (Smertenko *et al.*, 2004; Mao *et al.*, 2005b). Other GFP-tagged *At*MAP65 proteins have different localizations. *At*MAP65-3 is associated with the mitotic MT array during both early and late mitosis in all *Arabidopsis* organs (Caillaud *et al.*, 2008). *At*MAP65-4 associates with the prophase spindle MTs and labels the spindle MTs until anaphase (Van Damme *et al.*, 2004a). *At*MAP65-6 colocalizes with mitochondria (Mao *et al.*, 2005b). Finally, *At*MAP65-5 associates with a subset of transversely organized CMT bundles in interphase as well as the phragmoplast during cytokinesis (Van Damme *et al.*, 2004a). On the basis of the their diverse localization patterns, we postulate that *At*MAP65s exhibit differential molecular and functional properties which still remain to be identified.

In this report we investigated the molecular and functional properties of *At*MAP65-5 and further investigated biochemical mechanisms of *At*MAP65-1 MT binding and MT bundling. We found that in vivo AtMAP65-1 and *At*MAP65-5 differentially associate with MTs during prophase preceding the initiation and formation of a bipolar spindle and at the end of metaphase and during anaphase. In vitro, we demonstrate that *At*MAP65-1 and *At*MAP65-5 are monomeric in solution and promote the bundling of antiparallel aligned MTs. The presented data are in favor of their binding to MTs as monomers followed by their homodimerization through their N-terminal regions when adjacent MTs encounter.

MATERIALS AND METHODS

Recombinant Protein, Expression, and Purification

*At*MAP65-1 (At5g55230), *At*MAP65-5 (At2g38720), domains of *At*MAP65-1 and *At*MAP65-5, *At*MAP65-1, and *At*MAP65-5 deleted of one domain were purified as tagged proteins with either His tag at N- and C-termini, or GFP at the N-terminus and His tag at the C-terminus using homemade vectors. Primers used to amplify cDNAs are given in Supplemental Table S1.

For *At*MAP65-1 and *At*MAP65-5 three domains were defined: 1) for *At*MAP65-1: the domain 1 (aa 1-150), the domain 2 (aa 151-339), and the domain 3 (aa 340-587); for *At*MAP65-5: the domain 1 (aa 1-140), the domain 2 (aa 141-328), and the domain 3 (aa 329-550). These domains and *At*MAP65-5 or *At*MAP65-1 deleted of one domain were further referred to as *At*MAP65-5(1), *At*MAP65-5(2), *At*MAP65-5(3), and *At*MAP65-5(13) and as *At*M65-5(23), *At*MAP65-1(1), *At*MAP65-1(2), *At*MAP65-1(3), *At*MAP65-1(23), and AtMAP65-1(13). All sequences were verified by sequencing.

Recombinant *At*MAP65s proteins were purified on Ni Sepharose columns and stored at −80°C in 10% (vol/vol) glycerol, 50 mM NaPi, 0.1 M NaCl, and 0.5 mM DTT, pH 7.9. A detailed protocol is given in Supplemental Data.

Tubulin Polymerization and MT-binding Assays

Purified bovine tubulin (Vantard *et al.*, 1994) was assembled in G-BRB80 buffer (BRB buffer: 80 mM Pipes, pH 6.8, 1 mM EGTA, and 1 mM $MgCl_2$ plus 1 mM GTP). Polymerization was monitored at 350 nm at 37 or 4°C. For experiments using preformed MTs, MTs were assembled from 20 μM tubulin in presence of 20 μM of taxotere (Sigma, St. Louis, MO) in G-BRB80 at 37°C for 30 min and further diluted in G-BRB80 supplemented with 10 μM taxotere. MTs were incubated with *At*MAP65s at 20°C for 20 min. For cosedimentation assays, reaction mixtures were spun (10 min, 100,000 × *g*) through a glycerol cushion (30% [vol/vol] glycerol in G-BRB80 plus 10 μM taxotere). Supernatants and pellets were analyzed on western blot probed with anti-*At*MAP65-1 or anti-*At*MAP65-5 antibodies. For analyses of the relative efficiencies of full-length and constructs of *At*MAP65s to bundle MTs, cosedimentation assays were done at low-speed centrifugation (10 min, 4000 × *g*).

Imaging Assays

Fluorescent MTs assembled from a mixture of 5 μM rhodamine-labeled tubulin (prepared according to Hyman *et al.*, 1991) and 10 μM unlabeled tubulin were incubated at 20°C with *At*MAP65s and observed according to Stoppin *et al.* (1996).

For *At*MAP65s binding on MTs, rhodamine MTs (0.2 μM) were incubated for 5 min with GFP-*At*MAP65s (0.5 μM), and a 1-μl sample was observed on fluorescence microscope (Axioplan 2 microscope, 63× NA 1.3 objective; Zeiss, Thornwood, NY) and a Hamamastu CCD Orca camera (Bridgewater, NJ) and Metaview image processing (Molecular Devices, Downingtown, PA).

For negative-stain electron microscopy (EM) observations, MTs (1 μM) were incubated at 20°C for 20 min with *At*MAP65s (1 μM). Samples were stained with 2% (wt/vol) uranyl acetate and observed on a CM12 microscope (FEI, The Netherlands, Eindhoven) operating at 120 kV. The polarity of MTs within bundles was determined by cryo-EM as described by Chrétien *et al.* (1996). With this method MTs show fringe patterns produced by the superposition of protofilaments from the front and back of the MT wall in projection. To increase the contrast of fringes observed in vitrified MTs images, we computed filtered images using the J_0 and J_N terms in the Fourier transform of the images. Arrowhead patterns formed by the dark fringes are then clearly visible on these filtered images.

These differences between the values (inter-MT distance, cross-bridges angles) calculated from negative-stain EM or cryo-EM micrographs are inherent to the two methods of sample preparation for EM and are explained by the fact that with negative staining procedure, we only observe surface information (the footprint of the object in the stain). Furthermore after this procedure, MT bundles may be flattened, whereby errors are introduced that account for an apparent shorter inter-MT distance and a smaller angle. On the other hand, the cryo-EM method preserves much better the native form and the structure of the specimen (Dubochet *et al.*, 1988), and images contain information all along the thickness of the vitreous sample, contributing thus to a larger distribution of MT interspace lengths. Via cryo-EM, a projection of a 3D object is obtained, allowing the calculation of internal positional information of the specimen (see Figure 9B). Because the specimen preparation procedure preserves better the original structure, data are more reliable.

Oligomerization Determination

Analytical ultracentrifugation sedimentation velocity experiments were performed at 20°C and 42,000 rpm in two channel centerpiece cells loaded in a rotor ANTi50 in a Beckman XLI (Fullerton, CA). Samples were obtained from gel filtration eluted with 10% glycerol, 0.1 M NaCl, 0.5 mM DDT, and 50 mM NaPi, pH 8. Scans were recorded overnight at 280 nm. Analysis, done with the program Sedfit (available free at www.analyticalultracentrifugation.com), were performed in terms of continuous distribution, c(s), of sedimentation coefficients, s,(Ebel, 2007) and in terms of noninteracting species allowing the independent determination of s and molecular weight (MW; Schuck, 2000). Equations for calculation of $s_{20,w}$ and MW are given in Supplemental Data. The disordered regions were determined using the DisEMBL1.5 software (http://dis.embl.de/).

Polyclonal Antibody Production and Purification

Recombinant purified *At*MAP65-1 and *At*MAP65-5 were used as antigens to raise antibodies. Antisera were produced at a commercial facility (Charles River Laboratories, Wilmington, MA). IgG was isolated from the antisera by the method described by Vantard *et al.* (1994).

In Vivo Confocal Imaging

*At*MAP65-1-GFP, AtMAP65-5-GFP, and red fluorescent protein (RFP)-TUA6 constructs are already described (Van Damme *et al.*, 2004a). *At*MAP65-GFP constructs were supertransformed into a BY-2 suspension culture stably expressing RFP-TUA6 as described (Geelen and Inzé, 2001). The BY-2 cells were imaged using a chambered coverglass system (Labtek, Nunc, Naperville, IL) and immobilized in BY-2 medium with added vitamins and 0.8% of low melting point agarose (Invitrogen, Carlsbad, CA). Images were captured on using a 60× water corrected lens with an NA of 1.2 and 3× zoom on an Olympus Fluoview 1000 inverted confocal microscope, with standard en-

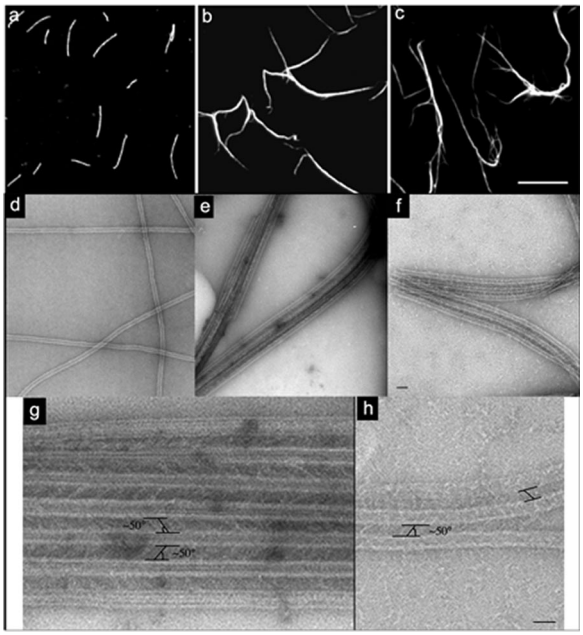

Figure 1. AtMAP65-5 bundles MTs in vitro. (a–c) Observations of rhodamine-labeled taxol-stabilized MTs (1 μM) incubated in the absence (a) or in the presence of *At*MAP65-5 (b) and *At*MAP65-1 (c) at 0.5 μM. *At*MAP65-1 and *At*MAP65-5 induce MT bundling. Scale bar, 10 μm. (d–h) Negatively stained electron microscopy of MTs alone (d), with *At*MAP65-5 (e and g) and with *At*MAP65-1 (f and h). Low-magnification view of MTs and bundled MTs (d, e, and f, respectively). Scale bar, 75 nm. (g and h) High-magnification view of aligned MTs shows *At*MAP65-5 (g) and *At*MAP65-1 (h) forming extensive inter-MT bridges oriented with an angle of ~50° relative to the axis of the MTs. Scale bar, 50 nm.

hanced GFP (eGFP) and monomeric RFP (mRFP) settings (15% 488-nm Argon laser power, 15% 559-nm diode laser power; DM405/488/559/635 excitation filter, SDM 560 beam splitter; 500–545-nm emission window for eGFP and 570–670-nm emission window for mRFP) using consecutive line capturing mode and four times Laman line averaging. 3D reconstruction was performed using the 3D software module of the FV1000 software.

RESULTS

AtMAP65-5 Cross-Link MTs in a Fishbone Pattern

When *At*MAP65-5 was incubated with rhodamine-labeled MTs, MT bundles were observed (Figure 1b). As already reported, *At*MAP65-1 produced similar MT bundles (Figure 1c; Smertenko *et al.*, 2004). *At*MAP65-5 and *At*MAP65-1 were both localized along the entire length of the bundles (Supplemental Figure S1). Electronmicrographs of *At*MAP65-5–induced bundles show that MTs are parallel-arranged and separated by cross-bridges at an average distance of 25 nm (Figure 1e). The cross-bridges form a lattice that is equally spaced along the MT walls and diagonally oriented between two adjacent parallel MTs. The angle between the cross-bridges relative to the MT axis was 50° on average (n = 95; Figure 1g). Comparable data were obtained with *At*MAP65-1 (Figure 1, f and h) as described for carrot MAP65-1 by Chan *et al.* (1999).

AtMAP65-5 and AtMAP65-1 Bundle MTs through Their N-terminal Part

To locate the domains of *At*MAP65-5 and *At*MAP65-1 required for MT bundling and cross-bridge formation, we defined three different domains on the basis of the amino acid sequence

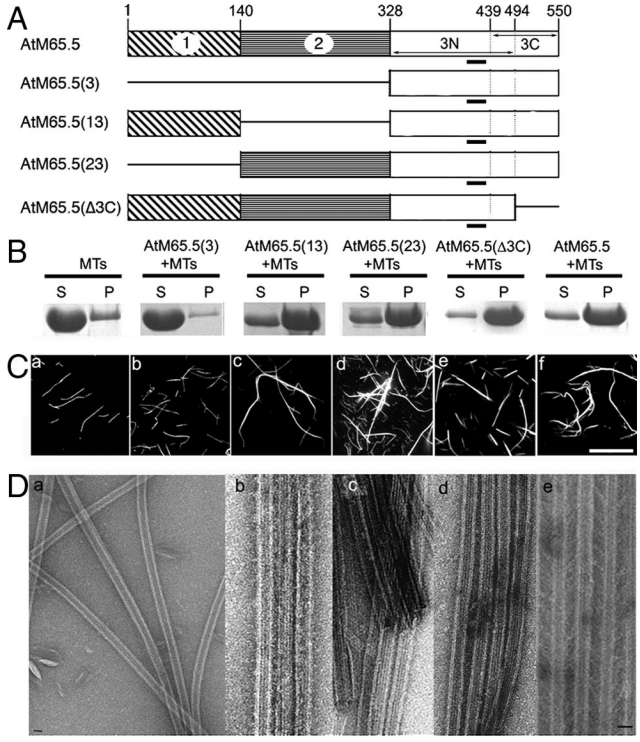

Figure 2. Analysis of functional domains of *At*MAP65-1 on MT bundling in vitro. (A) Diagrams of the *At*MAP65-1 domains and their combinations. The conserved motif through evolution is underlined. (B) Bundled MTs and individual MTs were separated by low-speed centrifugation. *At*MAP65-1 proteins at 5 μM were incubated with 1 μM of MTs. Pellets (P) and supernatants (S) were separated on SDS-PAGE. (C) Rhodamine-labeled taxol-stabilized MTs were incubated in the absence (a) or in the presence of *At*MAP65-1(3) (b), *At*MAP65-1(13) (c), *At*MAP65-1(23) (d), *At*MAP65-1(Δ3C) (e), and *At*MAP65-1 (f). Scale bar, 20 μm. (D) Negatively stained electron microscopy: MTs alone (a) and incubated with *At*MAP65-1(13) (b), *At*MAP65-1(23) (c), AtMAP65-1(Δ3C) (d), and *At*MAP65-1 (e). *At*MAP65-1(13), *At*MAP65-1(23), and *At*MAP65-1(Δ3C) induce MT bundles. The distance separating MTs in bundles induced by the (13) or (23) domains is smaller than 10 nm, whereas the distance between two adjacent MTs within bundles induced by *At*MAP65-1 or *At*MAP65-1(Δ3C) is 25–30 nm. Scale bar, 25 nm.

alignment of the *At*MAP65s (Figures 2 and 3). Roughly the domains correspond to the N-terminal, the central and the C-terminal regions of the *At*MAP65-5 and *At*MAP65-1 proteins (referred as to domains 1, 2, and 3, respectively). In addition, the domain 3 (C-terminal region) was subdivided in two domains: the N-terminal part including the most evolutionarily conserved domain of MAP65 family (referred as to 3N) and the C-terminal part, which is divergent among the *At*MAP65 members (referred as to 3C). The separate fragments as well as combinations thereof, were purified as His-tagged recombinant proteins [designated *At*MAP65(2), *At*MAP65(3), *At*MAP65(13), *At*MAP65(23), *At*MAP65(3N), *At*MAP65(3C), and *At*MAP65(Δ3C); Figures 2A and 3A].

High speed centrifugation of both *At*MAP65s and their different constructs [*At*MAP65(2), *At*MAP65(3), *At*MAP65(13), *At*MAP65(23), *At*MAP65(Δ3C), and *At*MAP65(3C)] after incubation with MTs led to the sedimentation of the proteins carrying the domain 3N of either *At*MAP65-5 or *At*MAP65-1 (Supplemental Figure S2). The proteins *At*MAP65(2) and *At*MAP65(3C) did not sedimented with MTs. These results indicate that the MT-binding domain of *At*MAP65-5 and

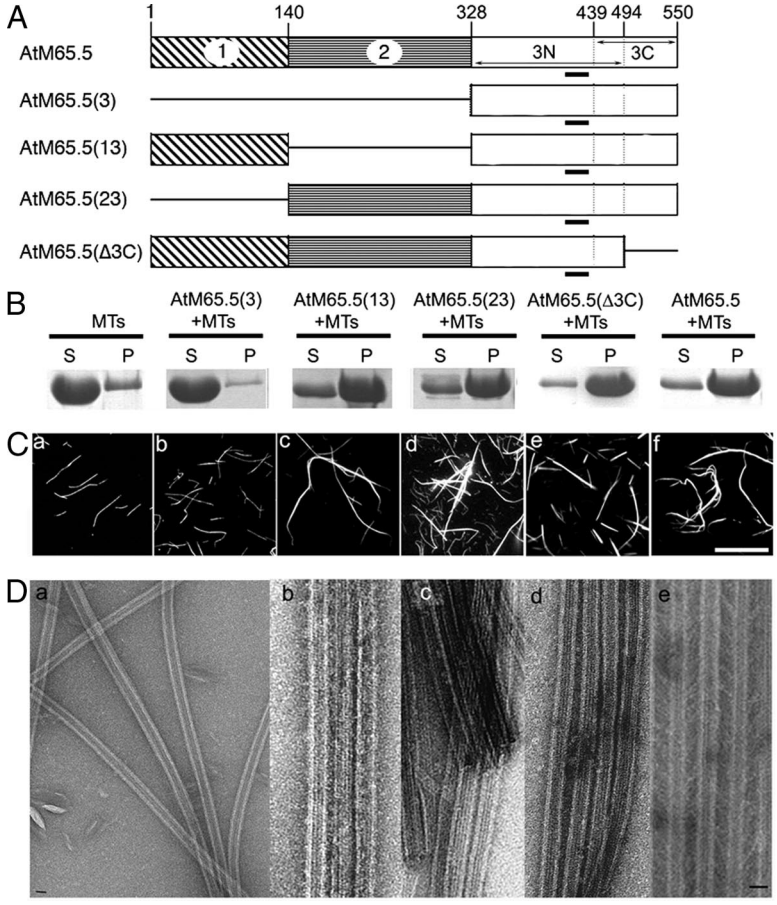

Figure 3. Analysis of functional domains of *At*MAP65-5 on MT bundling in vitro. (A) Diagrams of the *At*MAP65-5 domains and their combinations. The conserved motif through evolution is underlined. (B) Bundled MTs and individual MTs were separated by low-speed centrifugation. *At*MAP65-5 proteins at 5 μM were incubated with 1 μM MTs. Pellets (P) and supernatants (S) were separated on SDS-PAGE. (C) Rhodamine-labeled taxol-stabilized MTs were incubated in the absence (a) or in the presence of *At*MAP65-5(3) (b), *At*MAP65-5(13) (c), *At*MAP65-5(23) (d), *At*MAP65-5(Δ3C) (e), and *At*MAP65-5 (f). Scale bar, 20 μm. (D) Negatively stained electron microscopy: MTs alone (a) and incubated with *At*MAP65-5(13) (b), *At*MAP65-5(23) (c), *At*MAP65-5(Δ3C) (d), and *At*MAP65-5 (e). *At*MAP65-5(13), *At*MAP65-5(23), and *At*MAP65-5(Δ3C) induce MT bundles. The distance separating MTs in bundles induced by the (13) or (23) domains is smaller than 10 nm, whereas the distance between two adjacent MTs within bundles induced by *At*MAP65-5 is 25–30 nm. (Dd) shows that *At*MAP65-5(Δ3C) induces a distance separating MTs smaller than 10 nm. Scale bar, 25 nm.

*At*MAP65-1 is located in the domain 3N corresponding to the conserved part of the C-terminal domain of these two MAPs, in agreement with previous reports on MAP65 members (Mollinari *et al.*, 2002; Smertenko *et al.*, 2004; Loïdice *et al.*, 2005).

The efficiency of MT bundling by the different *At*MAP65 proteins was assayed by low-speed centrifugations that allow single MTs to remain in the supernatant, while bundled MTs sediment. Analysis of the supernatant and pellets (Figures 2B and 3B) showed that the MTs cosedimented with the constructs *At*MAP65(13), *At*MAP65(23), and *At*MAP65(Δ3C) but not with *At*MAP65(3). These results demonstrate that the N-terminal and the central domain of both *At*MAP65-1 and *At*MAP65-5 are independently able to promote MT bundling in vitro, that the domain 3, carrying the MT-binding domain (3N), is not able by itself to induce microtubule bundling, and that the domain 3C (C-terminal domain) is not required for such activity.

Observations of rhodamine-labeled MTs incubated with *At*MAP65(13), *At*MAP65(23), and *At*MAP65(Δ3C) (Figures 2C and 3C) confirmed the cross-linking activity of the N-terminus and the central domains independently from each other. Measurements at the EM level of the distance between MTs into bundles (Figures 2D and 3D) showed that the inter-MT space was narrower in the presence of *At*MAP65 fragments than with the full-length *At*MAP65-1 and *At*MAP65-5 ($<$10 vs. $\sim$ 20–30 nm) except for *At*MAP65-1(Δ3C), which induced the same inter-MT spacing than full-length *At*MAP65-1 (Figure 2Dd).

These results suggest that the length of the proteins upstream of the MT-binding domain is determinant for the interspacing between MTs within bundles. Noticeably, even if the domain 3C of *At*MAP65-5 does not interact with MTs, it might play a role in the conformation of the binding domain because the distance between MTs in the presence of full-length *At*MAP65-5 is at two times longer than for *At*MAP65-5(Δ3C).

Soluble AtMAP65-5 and AtMAP65-1 Are Monomeric and Display Conformational Flexibility

The EM observations of MT bundles induced by *At*MAP65-5 and *At*MAP65-1 full-length proteins and the different fragments suggested that the inter-MT space depended on the protein size. As the measured distances for the full-length proteins of 20–40 nm on average are too large for a single protein to cover, oligomerization of the MAP65s was suspected. Therefore, we determined their degree of oligomerization in solution by sedimentation velocity (SV) analytical ultracentrifugation and size exclusion chromatography. The sedimentation coefficient (s_{20w}) of *At*MAP65-1 at 8 and 30 μM and of *At*MAP65-5 at 9 μM were 3.7 $\pm$ 0.25 S (Figure 4A). The calculated theoretic $s_{20,w}$ values for hydrated globular compact monomers of *At*MAP65-1 is 4.7 and 5 S for *At*MAP65-5, i.e., significantly larger than experimental values. The MW was roughly estimated from SV boundary spreading to be 60 kDa for the two proteins, in agreement with the predicted values of 65 and 73 kDa for *At*MAP65-1 and *At*MAP65-5, respectively. The results indicate that *At*MAP65-1 and *At*MAP65-5 are monomeric in solution and that they adopt extended conformations. The hydrodynamic radii (R_H) of *At*MAP65-1 and *At*MAP65-5 were calculated to be 42 and 46Å, respectively, corresponding to a frictional ratio f/f_{min} of $\sim$1.6. SV experiments with the different

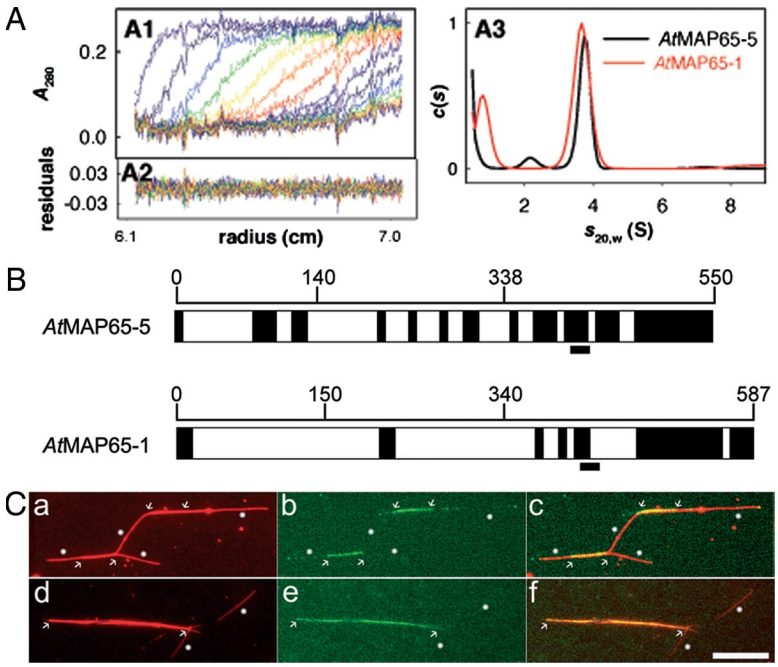

Figure 4. Determination of the oligomerization degree of *At*MAP65-1 and *At*MAP65-5. (A) Sedimentation velocity analytical ultracentrifugation of purified recombinant *At*MAP65-1 and *At*MAP65-5. (A1) Superimposition of selected experimental and modeled profiles obtained every hour with *At*MAP65-5 (9 μM). (A2) Residuals. (A3) c(s) of *At*MAP65-5 (9 μM) and *At*MAP65-1 (8 μM). (B) Disordered domains (dark boxes) of *At*MAP65-1 and *At*MAP65-5. The conserved motif through evolution is underlined. (C) Rhodamine-labeled taxol-stabilized MTs were perfused with GFP-*At*MAP65-1 (a–c) or GFP-*At*MAP65-5 (d–f). (a and d) Rhodamine channel, (b and e) GFP channel and (c and f) merge images. GFP-*At*MAP65-1 or GFP-*At*MAP65-5 accumulated along bundled MTs (delimited by arrows), whereas no significant accumulation of the protein were detected on nonbundled or single MTs (white dots). For example, GFP-*At*MAP65-5 did not accumulate on the two isolated MTs shown in panel d. Scale bar, 10 μm.

*At*MAP65 peptides provided s-values corresponding as well to monomers with f/f_{min} of ~1.5 (unpublished data).

Gel filtration chromatography showed an apparent MW in a range of 500 kDa for both *At*MAP65-5 and *At*MAP65-1, much larger than the expected ~70 kDa. Likewise, *At*MAP65 fragments produced apparent molecular sizes exceeding the values predicted from sequence data. As proteins with a high intrinsic disorder tend to show reduced mobility in gel-filtration columns (Receveur-Bréchot *et al.*, 2006) and because the experimentally determined MWs deviated from the predicted values, we suggest that *At*MAP65-5 and *At*MAP65-1 are possibly disordered and might adopt an elongated shape in solution. Indeed, according to their hydrodynamic properties (R_H = ~45Å, f/f_{min} = ~1.6), *At*MAP65-1 and *At*MAP65-5 behaved as random coils (Uversky, 2002). Using DisEMb1 software (Linding *et al.*, 2003), several disordered domains in *At*MAP65-1 and *At*MAP65-5 sequences were identified (Figure 4B). Because disordered domains generally lack tertiary structure and fold only upon interaction with other proteins, the presence of such domains in *At*MAP65-5 and *At*MAP65-1 support the viewpoint that they undergo conformational changes upon interaction with microtubules, themselves, and/or regulatory proteins.

Having determined that in solution both *At*MAP65-1 and *At*MAP65-5 are monomeric and postulating that at least a homo-dimer may be necessary to bundle two MTs together, we considered that *At*MAP65-5 and *At*MAP65-1 may bind to MTs as monomers and that this binding is not stable until they interact with a partner localized to a parallel MT. To address this question, we incubated single MTs with GFP-tagged *At*MAP65-1 or *At*MAP65-5 (Figure 4C). We observed that GFP-*At*MAP65-1 and GFP-*At*MAP65-5 localized along the MT bundles (detected as thick MTs, arrows in Figures 4C, a and d), whereas no significant accumulation of either *At*MAP65-1 or *At*MAP65-5 along MTs could be detected (n = ~100).

AtMAP65-5 and AtMAP65-1 Promote the Bundling of Antiparallel MTs

A key issue of the organization of MT bundles is their polarity (Ehrhardt and Shaw, 2006). Here we determined the polarity of MTs within *At*MAP65-5– and *At*MAP65-1– induced bundles in vitro using cryo-EM as described by Chrétien et al. (1996). Observed in vitreous ice, MTs with skewed protofilaments show arrowhead moiré patterns, the origin of which is related to an asymmetry of the mass distribution of the tubulin molecules in the MT wall. The arrowheads point toward the plus end of MTs when protofilaments show a right-handed skew and toward the minus end of MTs when protofilaments show a left-handed skew. Cryo-EM observation of in vitro AtMAP65-1 and AtMAP65-5–induced MT bundles confirmed the diagonal cross-linking pattern between adjacent MTs as detected by classic EM (~60 ± 5° relative to the MT axis, n = 40; Figure 5, A, a and b, and B, a and b). The inter-MT space in *At*MAP65-1 bundles was in the range of 30–40 nm and was more regular in comparison to *At*MAP65-5 bundles, which displayed MT separations varying between 15 and 40 nm. Note that for technical reasons, values obtained with cryo-EM are different from those calculated from EM micrographs. This point is explained in details in *Material and Methods.* The moiré patterns of *At*MAP65-1– and *At*MAP65-5–bundled MTs showed that the orientation of adjacent MTs in bundles induced by *At*MAP65-1 or *At*MAP65-5 was antiparallel (17 and 38 MTs were analyzed, respectively, for *At*MAP65-1 and *At*MAP65-5; Figure 5, Ac and Bc). Because no parallel arranged MTs were detected that are connected via *At*MAP65-5 or *At*MAP65-1 cross-bridges, we conclude that these two *At*MAP65 specifically promote antiparallel bundling of MTs. A much more complete description of the methodology used is explained in detail in Supplemental Materials.

Further inspection of the diffraction patterns calculated from cryo-EM images revealed an additional regular patterning corresponding to the spacing between *At*MAP65-1 and *At*MAP65-5 cross-bridges in projection (Figures 5A, d and e, and B, d and e). The diffraction patterns are calculated from vitrified MT images, revealing an additional regular patterning at project ~80Å, corresponding to the spacing between *At*MAP65-1 and *At*MAP65-5 cross-bridges in projection. This spacing corresponds to the tubulin dimer repeat. Nevertheless this further regular patterning corre-

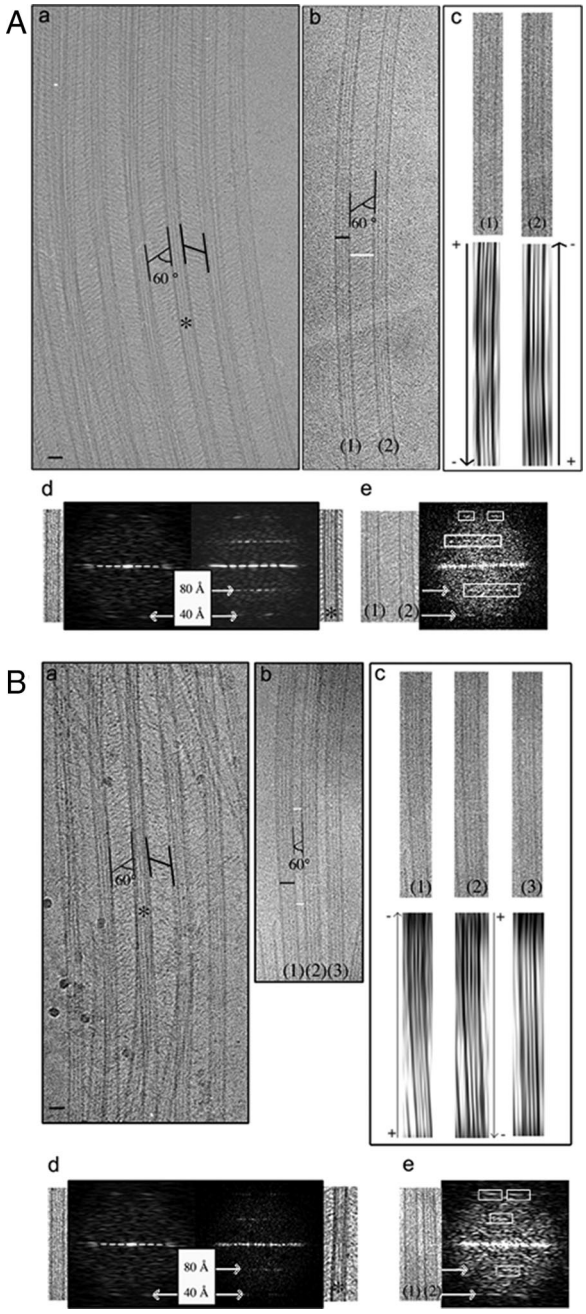

Figure 5. Determination of the polarity of MTs within bundles induced by *At*MAP65-1 and *At*MAP65-5. Cryo-EM of vitreous ice-embedded MTs incubated with *At*MAP65-1 (A) and *At*MAP65-5 (B). (Aa and Ba). View of aligned MTs showing *At*MAP65-1 and *At*MAP65-5 as extensive inter-MT bridges oriented with an angle of ~60° relative to the axis of MTs. (Ab) Two parallel MTs (1) and (2) separated by ~40 nm. Black and white scale bars represent 25 and 40 nm, respectively. (Ac) Associated filtered images of MTs (1) and (2). The direction of the arrowhead patterns is more clearly seen by looking obliquely along the MT axis. The arrowhead patterns point toward the minus end [bottom and top of the figure for the MTs (1) and (2), respectively], showing that MTs (1) and (2) are antiparallel. (Ad) Fourier transforms of an undecorated MT (left) and asterisk (*) indicates part of image a on right. Axial peaks at ~40Å spacing correspond to the axial rise between tubulin subunits (α- and β-tubulin are not distinguished at this resolution). Peaks at ~80Å spacing correspond to the tubulin dimer repeat and are visible only in the images of *At*MAP65-1–decorated MTs, indicating that one *At*MAP65-1 binds per tubulin heterodimer in projection. (Ae) Fourier transform of the cryo-EM image (Ab). The layer-line at 1/8 nm confirms the binding of *At*MAP65-1 to MTs. According to the diagonal orientation of *At*MAP65-1 relative to the axis of the MTs, peaks at ~80Å spacing are asymmetric. (Bb) Three parallel MTs (1), (2), and (3) separated by ~15–20 nm. Black and white scale bars, 25 and 18 nm, respectively. (Bc) Associated filtered images of MTs (1), (2), and (3). The third filtered image corresponds to a pattern of 13 protofilament MTs, whose polarity cannot be determined using moiré patterns. The arrowhead patterns point toward the minus end [top and bottom of the figure for the microtubules (1) and (2), respectively], showing that MTs (1) and (2) are antiparallel. (Bd) Fourier transforms of an undecorated MT (left) and asterisk (*) indicates part of image Ba on the right. Peaks at ~80Å are visible only in the images of *At*MAP65-5–decorated MTs, indicating that one *At*MAP65-5 binds to a tubulin heterodimer in projection. (Be) Fourier transform of a part of the cryo-EM image Bb. The layer-line at 1/8 nm confirms the binding of *At*MAP65-5 to MTs. The diagonal orientation of *At*MAP65-5 relative to the axis of the MTs gives asymmetric peaks at ~80Å spacing.

sponds to a feature through the thickness of the sample; thus we cannot conclude that we have one MAP65 bound per tubulin dimer (Figure 9A). In conclusion, these data show that the two ends of cross-bridges observed within MT bundles are linked to adjacent MTs, indicating that at least two MT-binding domains are necessary to link two adjacent MTs.

In Vitro Tubulin Assembly in the Presence of Recombinant AtMAP65-5 and AtMAP65-1

Besides the properties of *At*MAP65-1 and *At*MAP65-5 to bundle MTs, we further addressed whether *At*MAP65-5 could affect tubulin assembly in vitro. We quantified the amount of tubulin that polymerized in the presence of *At*MAP65-5 by high-speed cosedimentation assays (Figure 6A) and by time-lapse spectroscopy (Figure 6B; kinetic graphs are shown in Supplemental Figure S3). In both series of experiments, we observed an increased amount of tubulin in the presence of *At*MAP65-5, suggesting that *At*MAP65-5 has an effect on tubulin assembly. By imaging assays, rhodamine-labeled tubulin, assembly in the presence of *At*MAP65-5 showed few MT bundles and often aggregates associated with radiating MTs were observed (Figure 6Cb).

As there is a controversy concerning the effects of *At*MAP65-1 and its C-terminal part on tubulin assembly, we performed similar experiments with both full-length *At*MAP65-1 and the truncated protein *At*MAP65-1(Δ3C). We observed an increase in the amount of the polymerized tubulin in the presence of both *At*MAP65-1 and *At*MAP65-1(Δ3C) (Figure 6, A and B). *At*MAP65-1(Δ3C) had a comparable although reduced activity in tubulin polymerization in comparison with *At*MAP65-1. We noted that *At*MAP65-5(Δ3C) also has similar effects on tubulin assembly than *At*MAP65-5, with *At*MAP65-5(Δ3C) being slightly less efficient than the full-length protein (Figure 6B). No polymerization of tubulin in the presence of the domains 3, 3N, and 3C of *At*MAP65-1 was observed (unpublished data), in contrast to a recent report by Li *et al.* (2007b) or with the domain 3 of *At*MAP65-5. *At*MAP65-1 and *At*MAP65-1(Δ3C) on the other hand did stimulate MT bundling when incubated with tubulin (Figure 6C, d and e). Because *At*MAP65-1 and *At*MAP65-5 have been shown to protect CMTs from cold-induced depolymerization (Wicker-Planquart *et al.*, 2004; our unpublished data), we suggest that the effect on MT polymerization observed in vitro might be mainly due to a stabilization of the MTs. Overall the data suggest that the main activity of *At*MAP65-5 and *At*MAP65-1 is to induce

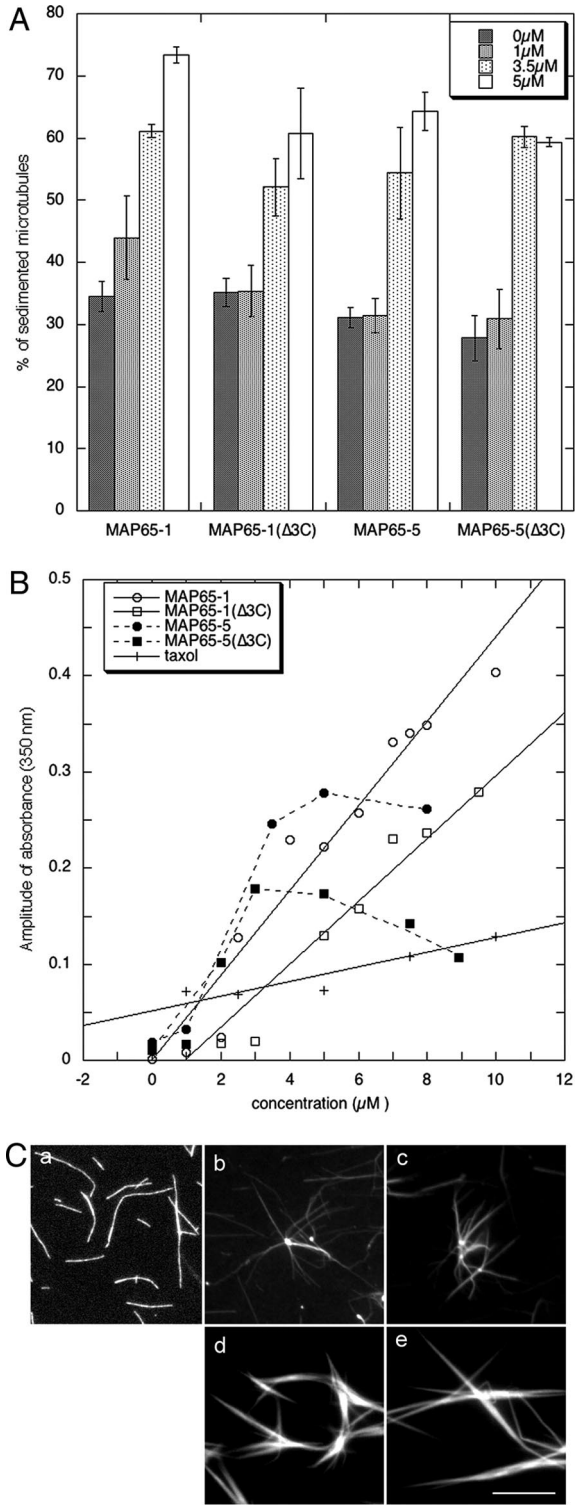

Figure 6. Effect of *At*MAP65-5 on MT assembly in vitro. (A) Quantification of the amount of tubulin (15 μM) that polymerized into MTs in presence of *At*MAP65s. MTs and associated *At*MAP65s were pelleted by high-speed centrifugation. (B) Tubulin assembly (15 μM) in presence of various *At*MAP65s concentrations was analyzed by turbidity assays. The amplitude of absorbance (Amax-A0) was plotted against the concentration of *At*MAP65s. Amax and A0 are obtained from kinetic curves shown in Supplemental Data (Supplemental Figure S3). (C) Rhodamine-labeled tubulin (15 μM) was assembled in the absence (a) or in the presence of 3.5 μM of *At*MAP65-5 (b), *At*MAP65-5(Δ3C) (c), *At*MAP65-1 (d), and *At*MAP65-1(Δ3C) (e). Scale bar, 10 μm

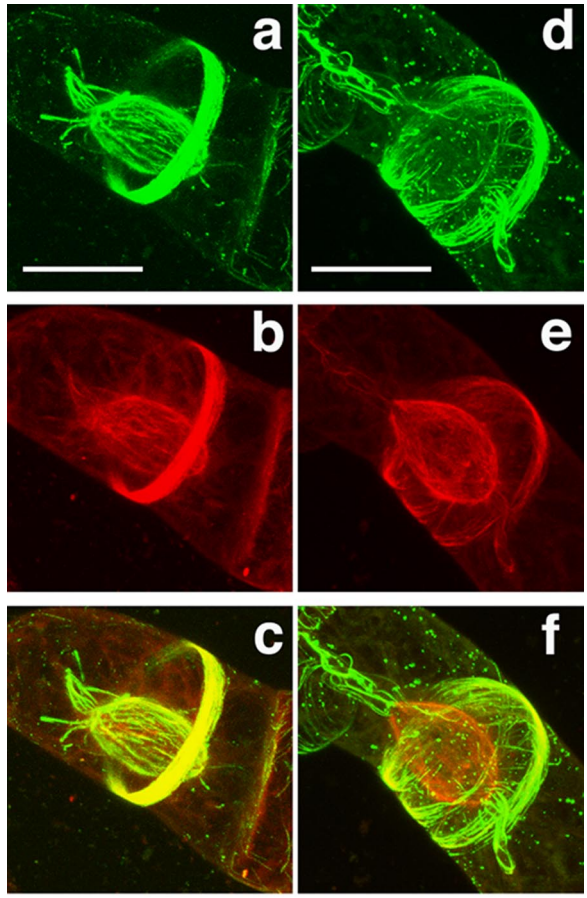

Figure 7. Differential localization of *At*MAP65-5 and *At*MAP65-1 during prophase. Tobacco BY-2 cells expressing *At*MAP65-5-GFP and RFP-TUA6 (A) and expressing *At*MAP65-1-GFP and RFP-TUA6 (B). Cells are observed in the GFP channel (a and d) and in the RFP channel (b and e), and images c and f are merged images of the RFP and GFP images (yellow signal; 3D reconstruction of confocal sections). *At*MAP65-5-GFP strongly accumulates at perinuclear MTs that initiate the formation of the spindle and at the preprophase band (A). *At*MAP65-1-GFP accumulates at the preprophase band but does not concentrate around the nucleus (B). Scale bar, 30 μm.

MT bundling but not to promote MT polymerization in vitro, in line with previous reports on *At*MAP65-1 and *Nt*MAP65-1 (Smertenko *et al.*, 2004; Wicker-Planquart *et al.*, 2004).

At*MAP65-5 Localization during Mitosis*

To study *At*MAP65-5 MT-binding properties in vivo, we followed its subcellular localization in transformed dividing BY-2 cells expressing *At*MAP65-5-GFP and compared it to the *At*MAP65-1 localization. Typically, during interphase CMTs were decorated with GFP-*At*MAP65-5 (Van Damme *et al.*, 2004a). We found that during prophase, GFP-*At*MAP65-5 strongly labeled the preprophase band, a hallmark for the division zone, and the perinuclear MTs before the initiation of the bipolar spindle (Figure 7A, Video S1). The perinuclear MTs labeled with *At*MAP65-5 are coaligned and formed a basket surrounding the nucleus. In some cells, at the polar sides of the cage, MTs emanate toward the distal ends of the cells. These aster-like MTs, when present, were labeled by *At*MAP65-5-GFP (Figure 7A). Upon nuclear envelope breakdown, *At*MAP65-5-GFP dissociated from the

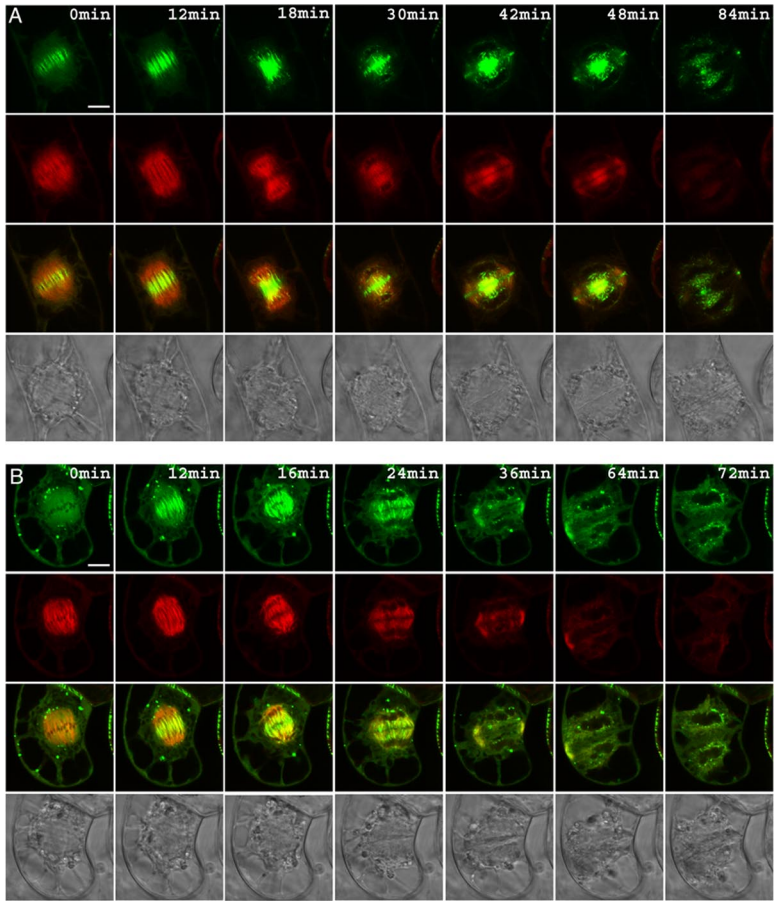

Figure 8. AtMAP65-5 accumulates in the midzone in metaphase until late anaphase. Time-lapse recording of tobacco BY-2 cells expression *At*MAP65-5-GFP and RFP-TUA6 (A) and *At*MAP65-1-GFP and RFP-TUA6 (B). The yellow signal in the third rows corresponds to the merged of RFP and GFP images. The rows at the bottom show differential interference contrast images. *At*MAP65-5 strongly labels the midzone from late metaphase until late anaphase and the phragmoplast in telophase (A). Conversely *At*MAP65-1 does not localized at the midzone during metaphase but appears at the onset of anaphase (B). Scale bar, 10 μm.

perinuclear MTs to reassociate with the interdigitated MTs at the spindle midzone at the end of metaphase until the end of anaphase (Figure 8A, Video S2). On initiation of the phragmoplast, *At*MAP65-5-GFP accumulated in the central zone, displaying discrete filamentous structures between the separating nuclei. A few minutes later when the phragmoplast flattened, *At*MAP65-5-GFP concentrated at a narrow zone in the center and at the side of the nucleus that faces the equatorial zone (this study; Van Damme *et al.*, 2004a). In comparison, *At*MAP65-1-GFP, that which colocalizes with the CMTs and the preprophase band (Van Damme *et al.*, 2004a; Smertenko *et al.*, 2004; Mao *et al.*, 2005a), was absent from the perinuclear area, but did associate with aster-like polar MT bundles when present (Figure 7B, Video S3). Furthermore, *At*MAP65-1-GFP showed a limited accumulation at the spindle midzone only in early anaphase (Figure 8B, Video S3), the labeling being stronger in late anaphase. These observations revealed that in vivo the MT binding of *At*MAP65-5-GFP is spatially and temporally regulated during the cell cycle and that its subcellular distribution during mitosis is partly different to that of *At*MAP65-1.

DISCUSSION

This report expands the analysis of the molecular properties of *At*MAP65-5 and provides uncovers previously unknown properties for *At*MAP65-1.

We found that *At*MAP65-5 induces MT bundling in vitro and that it binds MTs through the domain conserved among *At*MAP65s (referred as domain 3N), this domain alone being unable to induce MT bundling and tubulin assembly. Similarly we found that *At*MAP65-1 has only one MT-binding domain (within the domain 3N) and that this domain is not able to stimulate tubulin assembly and MT bundling.

*At*MAP65-5 and *At*MAP65-1 contain intrinsic disordered domains mostly within their C-terminal domain (domain 3) as suggested by Li *et al.* (2007a) for *At*MAP65-1. Disordered domains provide a level of structural plasticity by their propensity to form tertiary structure upon binding to physiological partner(s) (Gunasekaran *et al.*, 2003; Receveur-Bréchot *et al.*, 2006). *At*MAP65-5 appears more disordered than *At*MAP65-1, suggesting differences in their structure when bound to MTs or other physiological partner(s). Recently, Smertenko *et al.* (2006) showed that in vivo, the MT-binding activity of *At*MAP65-1 is partly controlled by phosphorylation of nine amino acid residues within its 3C-terminal domain and that phosphorylation weakens interaction of *At*MAP65-1 with MTs. Because it does not bind MTs in vitro and is highly disordered, it is possible that upon phosphorylation the 3C-terminal domain is refolded so that the conformation of the 3N- terminal domain changes, resulting in the weakness of *At*MAP65-1 binding to MTs. Because only one of the nine phophorylable *At*MAP65-1's residues is conserved in *At*MAP65-5, the regulation of its MT binding might rely on an alternative mechanism.

At*MAP65-5 Localization Is Cell Cycle Specific*

*At*MAP65-5 was shown to associate with a subset of transversely organized CMTs and the phragmoplast (Van Damme *et al.*, 2004a). Our time-lapse analysis of *At*MAP65-

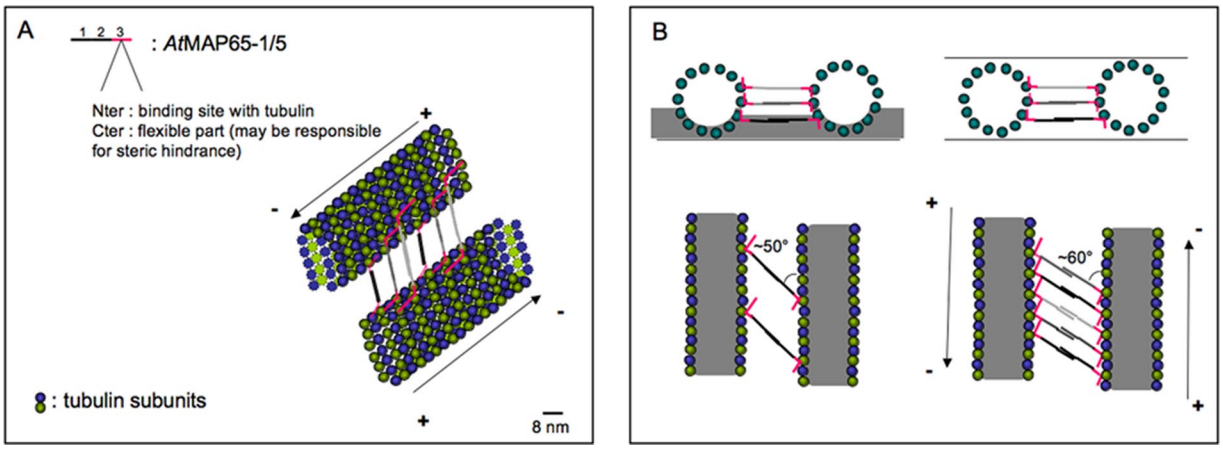

Figure 9. Schematic representation of *At*MAP65-5 or *At*MAP65-1 binding along the MT protofilaments. (A) Schematic view of MTs cross-linked by either *At*MAP65-5 or *At*MAP65-1. *At*MAP65-5 or *At*MAP65-1 dimerize via domains 1 and 2. The proximal region of domain 3 (red) binds to MTs. The distal region of this domain is unbound and may cause some steric hindrance. The cross-linked MTs are ~25–30 nm apart. (B) Schematic representation in negative stain and in vitreous ice (top left and right, respectively). Negative stain only partially embeds the cross-linked MTs (side view, above left) and consequently only one level of *At*MAP65-1 or *At*MAP65-5 is visible in the projected image (below) giving an observed spacing of ~24 nm. In vitreous ice, the ice specimen is fully embedded (side view, above right). In projection (below) the cross-linking molecules attached to different protofilaments are visible giving the observed repeat of 8 nm. MTs are in gray with outer border represented by tubulin subunits. Scale bar, 8 nm.

5's localization shows that during prophase, *At*MAP65-5 localizes at the perinuclear area at the onset of spindle formation and at the preprophase band. In comparison, *At*MAP65-1 does not associate with the perinuclear array, whereas within the same cell, it does bind the preprophase band. After nuclear envelop breakdown, *At*MAP65-5 reappears and labels distinct MTs in the spindle midzone not labeled by *At*MAP65-1. These observations indicate that the *At*MAP65-1 and *At*MAP65-5 MT-binding capacity might be controlled locally and temporally during mitosis.

MT Organization within Bundles Induced by AtMAP65-5 and AtMAP65-1

Using cryo-EM, we observed that in vitro MT bundles induced by *At*MAP65-5 and *At*MAP65-1 contain coaligned MTs 15–40 and 30–40 nm apart, respectively. This distance is in range of the inter-MT space reported for bundles at the cell cortex (Hardham and Gunning, 1978) and for carrot MAP65-1 and *At*MAP65-1 in vitro (Chan *et al.*, 1999; Smertenko *et al.*, 2004). Cross-bridges form a diagonal pattern connected with the MT wall at ~60° relative to the MT axis. Via cryo-EM, a projection of a 3D object is obtained, allowing the calculation of internal positional information of the specimen (Figure 9B). We calculated that *At*MAP65-5 or *At*MAP65-1 binds with a periodicity of 24 nm along the MT protofilaments, i.e., one molecule per three tubulin heterodimers (Figure 9A).

Each of the two ends of cross-bridges are linked to adjacent MTs, indicating that at least two MT-binding domains are necessary to link two adjacent MTs. As the inter-MT space is too large for a single MAP65 molecule to cross, *At*MAP65-1 and *At*MAP65-5 must undergo oligomerization to form the cross-bridges. We suggest that a cooperative action of domains 1 and 2 is required to build this link because deletion of one of these domains reduces the inter-MT spacing by half. Cross-bridges generated by *At*MAP65-5 were less regular and shorter on average than those generated by *At*MAP65-1, suggesting different conformational organization of domain 1 and 2 in two MAP65s. The presence of many short disordered stretches within the domain 1 and 2 in *At*MAP65-5 and just one in domain 2 in *At*MAP65-1 might be responsible for a difference in cross-bridge length. Therefore, the structural basis of the *At*MAP65-1 and *At*MAP65-5 interactions to induce MT bundling may be different for *At*MAP65-1 and *At*MAP65-5.

*At*MAP65-1 and *At*MAP65-5 behaved as monomers in their soluble forms. This result challenges the findings by Smertenko *et al.* (2004), who proposed that *At*MAP65-1 form homodimers in solution. Their conclusions were based on chemical cross-linking, native acrylamide gel electrophoresis and affinity chromatography with cell extracts. In view of the presence of disordered domains and high structural flexibility, we postulate that *At*MAP65-1 and *At*MAP65-5 dimerization is stimulated at high concentrations or when in contact with a protein-binding matrix. In addition, reduced electrophoretic migration in acrylamide gels is a common feature for unfolded proteins (Receveur-Bréchot *et al.*, 2006).

One possible interpretation of our results is that *At*MAP65-1 and *At*MAP65-5 bind to MTs as monomers and that this binding is not stable until they interact with a partner at an adjacent MT. This hypothesis is supported by the fact that in cryo-EM, no filament of *At*MAP65-1 or *At*MAP65-5 is seen projecting free from a single MT. In fluorescence assays, *At*MAP65-1 and *At*MAP65-5 accumulated along MT bundles but not along single MTs (Figure 4C). In comparison, in fission yeast binding of Ase1p to MTs is reinforced when Ase1p binds overlapped MTs (Janson *et al.*, 2007). In vivo, Van Damme *et al.* (2004a) reported that *At*MAP65-1-GFP or *At*MAP65-5-GFP associated with coaligned MTs and suggested that *At*MAP65-1-GFP may not bind to single MTs. Together, these data suggest a mode of action for *At*MAP65s MT bundling that involves the binding of monomeric *At*MAP65-5 and *At*MAP65-1 to MTs that zipper up through the homodimerization of the N-terminal regions when adjacent MTs encounter.

AtMAP65-5 and AtMAP65-1 Induce MT Bundling of Antiparallel MTs in Vitro

The polarity of MTs within a bundle remains a controversial issue. MTs were shown to polymerize within bundles in two directions, suggesting an antiparallel organization (Chan *et*

al., 2003; Shaw *et al.*, 2003; Van Damme *et al.*, 2004b; Vos *et al.*, 2004), whereas Dixit *et al.* (2006) reported that the majority of cortical MTs have the same polarity and that the polar arrangement of CMTs occurs simultaneously with parallel MT arrangement. Using the hook decoration, Tian *et al.* (2004) showed that the polarity of MTs in the cortical array is not uniform. In the present study, we provide by an original way new evidence that *At*MAP65-1 and *At*MAP65-5 stimulate antiparallel bundling of MTs in vitro.

The subcellular localization of *At*MAP65-1-GFP and *At*MAP65-5-GFP further supports a preference for antiparallel MT bundling in vivo. During late metaphase and anaphase *At*MAP65-5 localizes to the midzone and *At*MAP65-1 during late anaphase where numerous nonkinetochore MTs are antiparallel overlapping MT plus ends. Noticeably, Ase1p has the inherent ability to distinguish between parallel and antiparallel MTs (Janson *et al.*, 2007). We propose a similar property for *At*MAP65-1 and *At*MAP65-5 but their ability to control the self-organization of MT bundles in plant cells remain to be addressed.

The question of how *At*MAP65-1 or *At*MAP65-5 regulate the polarity of MTs in plant living plant cells remains unsolved. Janson *et al.* (2007) demonstrated that Ase1p localizes to overlapping (−) ends during interphase and overlapping plus ends in the anaphase spindle, the difference in localization being determined by molecular motors as Klp2p (a minus-end–directed motor) mediates the sliding of newly nucleated MTs along antiparallel MT bundles. In plant cells, ATK5, a plus end tracking protein molecular motor (Ambrose *et al.*, 2005) preferentially localizes at regions of overlap between opposing interpolar MTs, suggesting an increased affinity for plus ends in an antiparallel orientation (Ambrose and Cyr, 2007). In vitro, ATK5 equally coaligns with parallel or antiparallel MTs. One can postulate that the orientation of MTs is determined by MAPs such as *At*MAP65s that stabilize CMT coalignment. It will be important to determine whether *At*MAP65-1 or *At*MAP65-5 can organize stable regions of MT overlap in combination with the activity of a motor such as ATK5.

ACKNOWLEDGMENTS

We thank Laurent Blanchoin (iRTSV) and François Parcy (iRTSV) for helpful discussions and advice and Olivier Bastien (iRTSV) for help with computing analysis of *At*MAP65 sequences. We thank Richard Wade for advice on microtubule polarity determination and for careful reading of the manuscript. D.V.D. is a postdoctoral fellow of the Research Foundation-Flanders. Most of this work was supported by the French CNRS and CEA.

REFERENCES

Ambrose, J., Li, W., Marcus, A., Ma, H., and Cyr, R. (2005). A minus-end-directed kinesin with plus-end tracking protein activity is involved in spindle morphogenesis. Mol. Biol. Cell *16*, 1584–1592.

Ambrose, J., and Cyr, R. (2007). The kinesin ATK5 functions in early spindle assembly in *Arabidopsis.* Plant Cell *19*, 226–236.

Caillaud, M. C. *et al.* (2008). MAP65-3 microtubule-associated protein is essential for nematode-induced giant cell ontogenesis in *Arabidopsis.* Plant Cell. Advanced online publication 8 February 2008; doi: 10.1105/tpc.107.057422.

Chan, J., Jensen, C. G., Jensen, L. C., Bush, M., and Lloyd, C. W. (1999). The 65-kDa carrot microtubule-associated protein forms regularly arranged filamentous cross-bridges between microtubules. Proc. Natl. Acad. Sci. USA *96*, 14931–14936.

Chan, J., Calder, G. M., Doonan, J. H., and Lloyd, C. W. (2003). EB1 reveals mobile microtubule nucleation sites in *Arabidopsis.* Nat. Cell Biol. *5*, 967–971.

Chan, J., Calder, G., Fox, S., and Lloyd, C. W. (2007). Cortical microtubule arrays undergo rotary movements in *Arabidopsis* hypocotyl epidermal cells. Nat. Cell Biol. *9*, 171–175.

Chrétien, D., Kenney, J., Fuller, S., and Wade, R. (1996). Determination of microtubule polarity by cryo-electron microscopy. Structure *4*, 1031–1040.

Dixit, R., and Cyr, R. (2004). Encounters between dynamic cortical microtubules promote ordering of the cortical array through angle-dependent modifications of microtubule behaviour. Plant Cell *16*, 3274–3284.

Dixit, R., Chang, E., and Cyr, R. (2006). Establishment of polarity during organization of the acentrosomal plant cortical microtubule array. Mol. Biol. Cell *17*, 1298–1305.

Dubochet, J., Adrian, M., Chand, J. J., Homo, J. C., Lepault, J., McDowall, A. W., and Schultz, P. (1988). Cryo-electron microscopy of vitrified specimens. Rev. Biophys. *21*, 129–228.

Ebel, C. (2007). Analytical ultracentrifugation. State of the art and perspectives. In: Methods in Protein Structure and Stability Analysis: Conformational Stability, Size, Shape and Surface of Protein Molecules, ed. V. Uversky and E. A. Permyakov, New York: Nova Science Publishers.

Ehrhardt, D. W., and Shaw, S. L. (2006). Microtubule dynamics and organization in the plant cortex. Annu. Rev. Plant Biol. *57*, 859–875.

Geelen, D. N., and Inzé, D. G. (2001). A bright future for the bright yellow-2 cell culture. Plant Physiol. *127*, 1375–1379.

Gunasekaran, K., Tsai, C., Kumar, S., Zanuy, D., and Nussinov, R. (2003). Extended disordered proteins: targeting function with less scaffold. Trends Biochem. Sci. *28*, 81–85.

Hardham, A. R., and Gunning, B. (1978). Structure of cortical microtubules in plant cells. J. Cell Biol. *77*, 14–34.

Hussey, P., Hawkins, T. J., Igarashi, H., Kaloriti, D., and Smertenko, A. (2002). The plant cytoskeleton: recent advances in the study of the plant microtubule-associated proteins MAP-65, MAP-190 and the *Xenopus* MAP215-like protein, MOR1. Plant Mol. Biol. *50*, 915–924.

Hyman, A., Dreschel, D., Kellog, D., Salser, S., Sawin, K., Steffen, P., Wordeman, L., and Mitchison, T. (1991). Preparation of modified tubulins. Methods Enzymol. *196*, 478–485.

Janson, M., Loughlin, R., Loïodice, I., Brunner, C., Nédelec, F., and Tran, P. T. (2007). Crosslinkers and motors organize dynamic microtubules to form stable bipolar arrays in fission yeast. Cell *128*, 357–368.

Li, H., Mao, T., Zhang, Z., and Yuan, M. (2007a). The AtMAP65-1 cross-bridge between microtubules is formed by one dimer. Plant Cell Physiol. *48*, 866–874.

Li, H., Yuan, M., and Mao, T. (2007b). AtMAP65-1 binds to tubulin dimers to promote tubulin assembly. J. Biochem. Mol. Biol. *40*, 218–225.

Linding, R., Jensen, L. J., Diella, F., Bork, P., Gibson, T. J., and Russell, R. B. (2003). Protein disorder prediction: implications for structural proteomics. Structure *11*, 1453–1459.

Lloyd, C. W. (1994). Why should stationary plants cells have such dynamic microtubules? Mol. Biol. Cell *5*, 1277–1280.

Loïdice, I., Staub, J., Getty, T. G., Hguyen, N. T., Paoletti, A., and Tran, P. T. (2005). Ase1p organizes antiparallel microtubule arrays during interphase and mitosis in fission yeast. Mol. Biol. Cell *16*, 1756–1768.

Mao, G., Chan, J., Calder, G., Doonan, J. H., and Lloyd, C. W. (2005a). Modulated targeting of GFP-AtMAP65-1 to central spindle microtubules during division. Plant Cell *43*, 469–478.

Mao, T., Jin, L., Liu, B., and Yuan, M. (2005b). Two microtubule-associated proteins of the *Arabidopsis* MAP65 family function differently on microtubules. Plant Physiol. *138*, 654–662.

Mollinari, C., Kleman, J. P., Jiang, W., Schoehn, G., Hunter, T., and Margolis, B. (2002). PRC1 is a microtubule binding and bundling protein essential to maintain the mitotic spindle midzone. J. Cell Biol. *157*, 1175–1186.

Murata, M., Sonobe, S., Baskin, T. I., Hyodo, S., Hasezawa, S., Nagata, T., Horio, T., and Hasebe, M. (2005). Microtubule-dependent microtubule nucleation based on recruitment of gamma-tubulin in higher plants. Nat. Cell Biol. *7*, 961–968.

Pastuglia, M., Azimzadeh, J., Goussot, M., Camilleri, C., Evrard, J. L., Schmit, A. C., Guerche, P., and Bouchez, D. (2006). Gamma-tubulin is essential for microtubule organization and development in *Arabidopsis.* Plant Cell *18*, 1412–1425.

Receveur-Bréchot, V., Bourhis, J. M., Uversky, V., Canard, B., and Longhi, S. (2006). Assessing protein disorder and induced folding. Proteins *62*, 24–45.

Schuck, P. (2000). Size-distribution analysis of macromolecules by sedimentation velocity ultracentrifugation and lamm equation modeling. Biophys. J. *78*, 1606–1619.

Schuyler, S., Liu, J. Y., and Pellman, D. (2003). The molecular function of Ase1p: evidence for a MAP-dependent midzone-specific spindle matrix. J. Cell Biol. *160*, 517–528.

Shaw, S. L., Kamyar, R., and Ehrhardt, D. W. (2003). Sustained microtubule treadmilling in *Arabidopsis* cortical arrays. Science *300*, 1715–1718.

Smertenko, A., Chang, H., Wagner, V., Kaloriti, D., Fenyk, S., Sonobe, S., Lloyd, C. W., Hauser, M., and Hussey, P. (2004). The *Arabidopsis* microtubule-associated protein AtMAP65-1, molecular analysis of its microtubule bundling activity. Plant Cell *16*, 2035–2047.

Smertenko, A. P., Chang, H. Y., Sonobe, S., Fenyk, S. I., Weingartner, M., Bogre, L., and Hussey, P. (2006). Control of the AtMAP65-1 interaction with microtubules through the cell cycle. J. Cell Sci. *119*, 3227–3237.

Stoppin, V., Lambert, A. M., and Vantard, M. (1996). Plant microtubule-associated proteins (MAPs) affect microtubule nucleation and growth at plant nuclei and mammalian centrosomes. Eur. J. Cell Biol. *69*, 11–23.

Tian, G. W., Smith, D., Gluck, S., and Baskin, T. I. (2004). Higher plant cortical microtubule array analyzed in vitro in the presence of the cell wall. Cell Motil. Cytoskelet. *57*, 26–36.

Uversky, V. N. (2002). What does it mean to be natively unfolded? Eur. J. Biochem. *269*, 2–12.

Van Damme, D., Van Poucke, K., Boutant, E., Ritzenthaler, C., Inzé, D., and Geelen, D. (2004a). In vivo dynamics and differential microtubule-binding activities of MAP65 proteins. Plant Physiol. *136*, 3956–3967.

Van Damme, D., Bouget, F. Y., Van Poucke, K., Inzé, D., Geelen, D. (2004b). Molecular dissection of plant cytokinesis and phragmoplast structure: a survey of GFP-tagged proteins. Plant J. *40*, 386–398.

Vantard, M., Peter, C., Fellous, A., Schellenbaum, P., and Lambert, A. M. (1994). Characterization of a 100-kDa heat-stable microtubule-associated protein from higher plants. Eur. J. Biochem. *220*, 847–853.

Verni, F., Somma, M. P., Gunsalus, C. K., Bonaccorsi, S., Belloni, G., Goldberg, M. L., and Gatti, M. (2004). Feo, the *Drosophila* homolog of PRC1, is required for central-spindle formation and cytokinesis. Curr. Biol. *14*, 1569–1575.

Vos, J. W., Dogterom, M., and Emons, A. M. (2004). Microtubules become more dynamic but not shorter during preprophase band formation: a possible "search-and-capture" mechanism for microtubule translocation. Cell Motil. Cytoskelet. *57*, 246–258.

Wasteneys, G. O., and Fujita, M. (2006). Establishing and maintaining axial growth: wall mechanical properties and the cytoskeleton. J. Plant Res. *119*, 5–10.

Wicker-Planquart, C., Stoppin-Mellet, V., Blanchoin, L., and Vantard, M. (2004). Interactions of tobacco microtubule-associated protein MAP651b with microtubules. Plant J. *39*, 126–134.

Zhu, C., Lau, E., Schwarzenbacher, R., Bossy-Wetzel, E., and Jiang, W. (2006). Spatiotemporal control of spindle midzone formation by PRC1 in human cells. Proc. Natl. Acad. Sci. USA *18*, 6196–6201.